TOPOLOGY OPTIMIZATION AND EXPERIMENTAL INVESTIGATION OF COLD PLATE HYDROTHERMAL PERFORMANCE

Yanzhao Cai[1], Chen Sun[1*], Jinbiao Chen[1], Wei Wang[1,2], Xiwei Tian[1], Sihao Qian[1], Xiaohui Wang[3]

[*1] Key Laboratory of Electronic Equipment Structure Design, Ministry of Education, Xidian University, Xi'an 710071, China

[2] Shannxi Key Laboratory of Space Solar Power Station System, Xidian University, Xi'an 710071, China

[3] R&D Department, China Academy of Launch Vehicle Technology, Beijing 100076, China

[*] Corresponding author; E-mail: sunchen636@163.com

To enhance the hydrothermal performance of cold plates, this study constructs a topology optimization framework that integrates conjugate heat transfer principles, aiming to maximize heat generation and minimize fluid flow dissipation. The robustness of the design is improved through the application of projection and density filtering techniques, with the projection intensity value incrementally increased via a parameter scanning method to bolster numerical convergence. The inlet and outlet distribution of the cold plate, aligned along its centerline, is determined through various target weight combinations, generating clear, continuous layouts. To further substantiate the effectiveness of the optimized configuration, a topology optimization design employing an objective function weighting factor of 0.7:0.3 is chosen to create the three-dimensional geometry of the cold plate. A parallel flow channel design, maintaining an identical fluid volume fraction and heat transfer boundary length, is introduced for comparative analysis. Moreover, performance indices such as surface temperature, pressure drop across the channel, average Nusselt number, and thermal resistance are assessed for two cold plates under varying inlet velocities. Both simulations and experiments indicate that the hydrothermal performance of the developed topological structure significantly surpasses that of the conventional parallel channel design, a disparity that amplifies with increasing inlet velocities.

Key words: *Cold plate; Topology optimization; Hydrothermal performance; Thermal design*

1. Introduction

Liquid cooling plates find extensive application across a variety of mechanical and electronic devices, including automobile engines, power battery plates, and communication base stations. An optimal geometric configuration of the flow channels plays a crucial role in enhancing heat transfer efficiency and, consequently, elevating the overall performance of the system [1, 2]. Recently, topology optimization methods have become recognized as highly flexible and efficient design tools for addressing conjugate heat transfer issues.

The topology optimization technique demonstrates the ability to determine the optimal path for heat dissipation autonomously [3, 4]. Matsumori *et al.* [5] addressed two types of design problems related and unrelated to heat sources and topology, respectively. They introduced an integral equation to maintain constant input power at the inlet and solved for the optimal channel distribution based on the density method. Sato *et al.* [6] developed a Pareto front exploration algorithm for bi-objective topology optimization problems that adaptively determined weighting coefficients and explored the relationship between flow resistance and heat transfer. Zhao *et al.* [7] introduced a cost-effective strategy by substituting the Navier-Stokes equations with a Darcy flow model. By applying pressure drop and minimum size constraints, they solved the conjugate heat transfer problem under turbulent conditions. To tackle thermal dissipation challenges in power devices, Liu *et al.* [8] conducted topology optimization to design five micro-channel structures with varying aspect ratios based on density to enhance the synergistic effect. Li *et al.* [9] optimized the distribution of liquid-cooled paths with various inlet and outlet arrangements using density-based topology optimization. The performance of liquid-cooled plates in thermal dissipation was investigated using simulations and experiments. Zhang *et al.* [10] applied topology optimization to the cooling design of supersonic engines to improve system stability under non-uniform conditions. Three-dimensional topology optimization research faces challenges related to computational complexity, algorithm efficiency, manufacturability, and nonlinear problems. To address this issue, Haertel *et al.* [11] optimized thermal resistance subject to constraints on heat generation and pressure drop using a pseudo-3D model to reduce computational costs. Yaji *et al.* [12] effectively addressed the challenges associated with designing 2D and 3D heat flow systems using the level set method. Additionally, they managed the complexity of flow paths by adopting a regularization method. Pei *et al.* [13] developed a pseudo-3D optimization framework composed of a flow design layer and a thermal conductive substrate layer to optimize forced air cooling heat sinks. In addition, topology optimization for transient thermal analysis has received increasing attention. Long *et al.* [14] proposed an efficient quadratic approximation method for multi-material transient thermal problems, which improves computational efficiency and reduces the number of iterations. Li *et al.* [15] verified the effectiveness of functional gradient constraints for solving transient topology optimization problems through numerical cases.

The design of liquid cooling channels faces the challenges of efficient thermal performance, design flexibility, and complex flow patterns. To address these challenges, this study introduces a density-based topology optimization for cold plates with inlet and outlet configurations distributed on the center line of the cold plate. The design approach aims to maximize heat transfer while minimizing pressure drop by coupling dual objective functions. The distinct topology structures of the flow channel are achieved, and the Pareto solution set for the dual-objective optimization problem is calculated. Furthermore, a parallel flow channel structure is designed for comparison with the optimized structure, maintaining identical heat transfer boundary lengths and fluid volume fractions. The hydraulic and thermal performance of the cold plates with these two types of flow channel structures is studied through numerical simulations. Finally, experiments on cold plate samples are conducted to verify the rationality of the proposed design.

2. Topology optimization design for cold plate

2.1. Concept of topology optimization for flow channel layout

When the flow channel structure is kept consistent in the direction normal to the horizontal plane, the cold plate design process can typically be simplified and treated as a two-dimensional problem. Figure 1 illustrates the topology optimization problem for the planar layout of the channel, encompassing the mixed design domain, fluid inlet and outlet, and physical boundary conditions. The characteristic dimension L of the inlet is 8 mm. To tackle this, a pseudo-density value denoted as γ, which corresponds to the density method, is assigned to each unit within the design domain. $\gamma = 0$ for solids and $\gamma = 1$ for fluids. The search for the optimized layout of the flow path evolves into resolving a topology optimization "0-1" problem to find the optimal solution by using γ as the design variable.

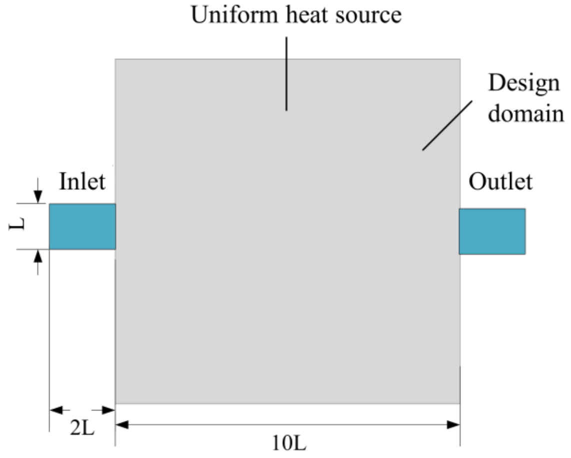

Fig. 1. Schematic representation of the design domain and the configuration of the inlet and outlet for the topology optimization problem.

2.2. Mathematical model construction

2.2.1 Governing equation for fluid flow

Considering the case of steady-state and incompressible Newtonian fluid flow, the characteristic length at the inlet serves as the basis for calculating the Reynolds number, which is defined as follows:

$$\mathrm{Re} = \frac{\rho U L}{\mu} \tag{1}$$

Fluid flow behavior can be described by the continuity and momentum equations. The continuity equation can be expressed as [16, 17]:

$$\nabla \cdot \mathbf{u} = 0 \tag{2}$$

The Navier-Stokes equation describes the movement of the viscous fluid, which is defined as [16, 17]:

$$\rho(\mathbf{u} \cdot \nabla)\mathbf{u} = -\nabla p + \nabla \cdot \left\{ \mu \left[\nabla \mathbf{u} + (\nabla \mathbf{u})^{\mathrm{T}} \right] \right\} + F \tag{3}$$

where ρ is the fluid density, $\mathbf{u}$ is the velocity field, and μ denotes the dynamic viscosity. F and p represent the body force and the pressure, respectively.

In thermal-fluid topology optimization, material distribution mimics porous media characteristics where fluid and solid phases coexist. Addressing fluid flow within porous media necessitates considering the additional drag experienced by the fluid during permeation through the material. A resistance term associated with fluid velocity is introduced into the momentum equation using the Brinkman penalty model [18]. The assumption is made that the resistance is generated by the opposing force that scales with the fluid velocity, and this relationship is represented by:

$$F = -\alpha \cdot \mathbf{u} \tag{4}$$

where α is the inverse permeability. When α is 0, it indicates that the porous media offers no resistance to fluid flow, enabling smooth fluid flow. Conversely, when α becomes infinitely large, the fluid is completely obstructed from passing through.

The rational approximation of material properties (RAMP) method is advantageous for its smooth interpolation of material properties, which enhances the efficiency and stability of the optimization process. Consequently, this study employs the RAMP method to achieve thermo-fluid topology optimization. The inverse permeability α is represented through a continuous function related to design variables, employing interpolation in the following manner:

$$\alpha(\gamma) = \alpha_{\min} + \left(\alpha_{\max} - \alpha_{\min}\right)\frac{q(1-\gamma)}{q+\gamma} \tag{5}$$

where q is the interpolation parameter that regulates the trend of the function $\alpha(\gamma)$. $\alpha_{\min}$ and $\alpha_{\max}$ represent the inverse permeability for the exclusive presence of solid and liquid phases, respectively. In the Brinkman penalty model, $\alpha_{\max}$ depends on the Darcy number (*Da*) and the magnitude of the viscous force, which is expressed as:

$$\alpha_{\max} = \frac{\mu}{Da \cdot L^2} \tag{6}$$

2.2.2 Governing equation for conjugate heat transfer

The governing equations for heat transfer in the solid and fluid domains are given as follows [3, 19, 20]:

$$k_s \nabla^2 T + Q = 0 \tag{7}$$

$$\rho C_p \left(\mathbf{u} \cdot \nabla\right) T = k_f \nabla^2 T + Q \tag{8}$$

where the thermal conductivity of the solid is denoted by k_s, and that of the fluid by k_f. C_p denotes the specific heat capacity. Q is the surface heat source, which can be defined by heat generation reliant on local temperature differences and is expressed by Newton's law of cooling:

$$Q = \eta\left(T_Q - T\right) \tag{9}$$

where η represents the heat generation coefficient that depends on the temperature difference. T represents the local temperature. T_Q denotes the prescribed temperature with a value of 80 ℃.

During the initial stages of topology optimization, it is often challenging to distinctly allocate the material properties of the solid and fluid components. To address this issue, the design variable γ is employed to consolidate the aforementioned equations into a single equation that describes the conjugate heat transfer process:

$$\gamma \rho C_p (\mathbf{u} \cdot \nabla) T = \left[(1-\gamma) k_s + \gamma k_f\right] \nabla^2 T + (1-\gamma) Q \tag{10}$$

2.2.3 Treatment of numerical instability

To circumvent numerical instability phenomena during topology optimization, a combined approach of density filter and projection methods is employed. The density filter is implemented using a Helmholtz-type partial differential equation, the expression of which is as follows [21]:

$$-r_{\mathrm{filter}}^2 \nabla^2 \tilde{\gamma} + \tilde{\gamma} = \gamma \tag{11}$$

where $\tilde{\gamma}$ and r_{filter} represent the filtered design variable and the filter radius, respectively.

The use of the density filter may introduce additional gray areas. To mitigate this, the Heaviside projection method is utilized in the optimization process to ensure a distinct channel structure [22]. The formulation is presented as follows:

$$\hat{\gamma} = \frac{\tanh(\beta \cdot \gamma_\beta) + \tanh\left(\beta \cdot \left(\gamma - \gamma_\beta\right)\right)}{\tanh(\beta \cdot \gamma_\beta) + \tanh(\beta \cdot (1.0 - \gamma_\beta))} \tag{12}$$

where γ_β represents the projection threshold, $\hat{\gamma}$ denotes the projection density, and β is the projection intensity. γ_β and β are set to 0.5 and 12, respectively. To ensure the convergence of optimization results, the projection control parameter β is set through a parameter scanning method, starting from an initial value of one and experiencing a twofold increase every thirty iterations until $\beta = 32$.

2.2.4 Modeling of multi-objective optimization problem

To comprehensively evaluate the effectiveness of a cold plate, two factors should be carefully considered: flow and heat transfer. Evaluation of the heat transfer performance involves analyzing the total heat generation occurring within the designated domain. Thus, maximizing heat transfer efficiency is equivalent to maximizing internal heat generation, as expressed by the equation:

$$J_{th} = \int_\Omega (1-\gamma)\eta(T_Q - T) d\Omega \tag{13}$$

where $1-\gamma$ ensures that heat is generated independently by the solids. The fluid primarily acts as a heat transfer medium. By confining heat generation to the solid components, the optimization can concentrate on channel structure design to improve heat transfer efficiency.

In addition, another objective involves minimizing fluid dissipation energy to enhance the flow characteristics of the cold plate and ensure smooth continuity of the flow path. This objective is defined by an integral-based objective function, expressed as follows:

$$J_f = \int_\Omega \left[\frac{1}{2}\mu \sum_{i,j} \left(\frac{\partial u_i}{\partial x_j} + \frac{\partial u_j}{\partial x_i} \right)^2 + \sum_i \alpha(\gamma) u_i^2 \right] d\Omega \tag{14}$$

After normalizing each objective, the weighting factors, denoted by w_1 and w_2, are used to combine the two objectives into a unified objective function, which can be formulated as the following:

$$J'_{th} = \frac{J_{th} - J_{th,\min}}{J_{th,\max} - J_{th,\min}}, \; J'_f = \frac{J_f - J_{\min}}{J_{f,\max} - J_{f,\min}} \tag{15}$$

The mathematical representation for topology optimization is presented below:

$$\begin{aligned} &\text{Find} && \gamma \\ &\text{Minimize} && J = -w_1 J'_{th} + w_2 J'_f \\ &\text{Subject to} && (2) - (12) \\ & && \frac{1}{V}\int_\Omega \gamma d\Omega - V^* < 0 \\ & && 0 \le \gamma \le 1 \end{aligned} \tag{16}$$

where V is the total volume of the domain. V^* is the maximum allowable volume fraction of the fluid. The constraints ensure a balanced distribution between the fluid and solid regions within the cold plate. Moreover, the constraints contribute to the stability and convergence of the optimization algorithm.

2.3. Numerical implementation of topology optimization

2.3.1 Implementation method

The described problem is implemented in COMSOL Multiphysics, which employs a finite element analysis approach. The solution of the convection-diffusion equation and the heat diffusion problem in the substrate are carried out using the heat transfer module [23]. The flow field analysis is conducted using the CFD module, where velocity and pressure are solved through second-order and first-order discretization, respectively. The direct sparse solver PARDISO provided by COMSOL Multiphysics is available for solving discrete finite element equations [24]. Fluid, heat transfer, and optimization variables are solved by separate solution procedures. The sensitivity analysis is carried out utilizing the adjoint variable method, owing to the invisible relationships between the objective function and design variables. The iterative algorithm adopts the method of moving asymptotes (MMA) for updating the variables [25]. The MMA algorithm shows significant advantages in topology optimization due to its efficient handling of nonlinear problems, rapid convergence, and applicability to large-scale problems. This approach can address various multi-physical topology optimization problems and is applicable across a wide range of scenarios. The convergence criterion is set to $\varepsilon = \left| J^{k+1} - J^{k} \right| \le 10^{-5}$.

2.3.2 Topology optimization results

Cold plates with consistent properties in the vertical direction are more advantageous for manufacturing. Additionally, research shows that at the height of the cold plate, the variations in the velocity field across different layers are relatively small [26]. Therefore, this study conducts topology optimization within a 2D design domain. Subsequently, the 2D result is extruded to create a 3D structure for numerical analysis. The topology optimization is carried out using the given parameters of Re = 100, η = 1×10^{6} [$\mathrm{Wm^{-2}K^{-1}}$]. By adjusting the weight coefficients of the objective function, multiple optimized cold plate flow channel topologies are obtained, as depicted in Fig. 2. Generally, the fluid enters the channel and divides into several main branches, which subsequently separate into smaller channels that resemble a “tree” distribution pattern. Finally, all branch channels converge into the main outlet channel, with a symmetric distribution of the final channel structure. Further analysis demonstrates that, when the objective of fluid pressure drop predominates in the optimization, there is a reduction in the number of independent solid domains and channel branches, alongside an increase in channel size. This effect arises because fewer branches and wider channels can significantly reduce the pressure drop loss inside the channels. As the weight of the heat transfer objective J_{th} gradually increases, the exclusive solid domains are further subdivided into smaller block domains, and the number of channels increases. Additionally, smaller branches emerge, and channels progressively envelop the entire design domain, ensuring sufficient heat transfer boundaries for effective heat exchange.

The variations in pressure drop ΔP and the length of the heat transfer boundary with the weighting factor of the two objectives are shown in Fig. 3. Observations reveal that the values of ΔP and the length of the heat transfer boundary are relatively small when the weighting factor is set to w_1:w_2 = 0.2:0.8. As the value of w_1:w_2 starts to increase, both parameter values exhibit a gradual increase. The trends in changes for both parameters are consistent, aligning with the observed conclusions.

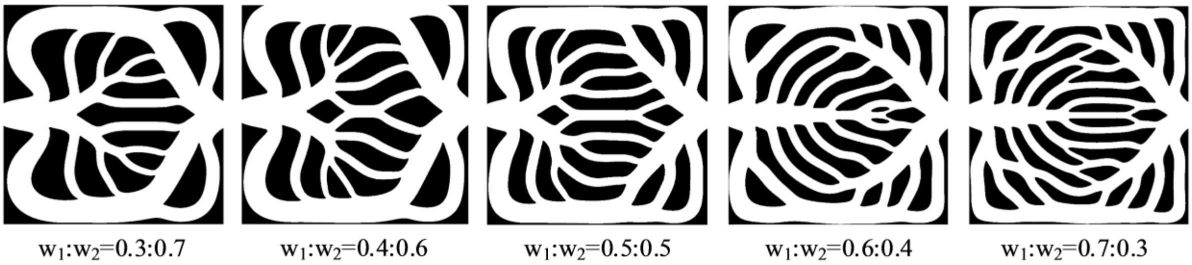

Fig. 2. Topology optimization structures of the flow channel under different weighting factors for multiple objectives.

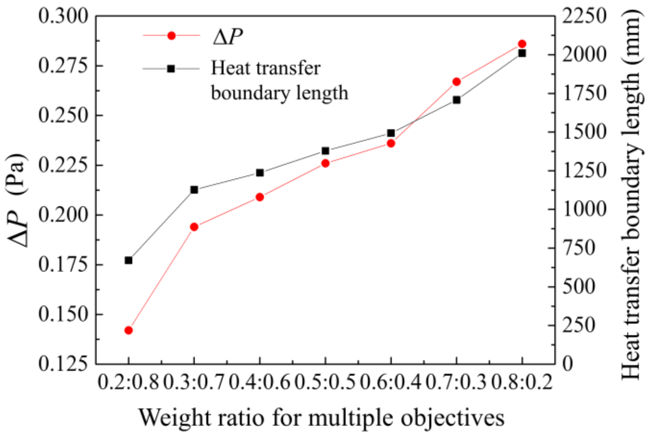

Fig. 3. Curves of pressure drop ΔP and heat transfer boundary length with changes in the weighting factor of the two objectives.

2.3.3 Pareto front for multi-objective optimization

In multi-objective optimization problems, the Pareto front provides a comprehensive solution space, facilitating the selection of an optimal solution based on specific requirements. A suite of optimal solutions is obtained by solving multiple sets of multi-objective optimization problems with distinct weighting factors. This approach enables the exploration of various trade-offs between different objectives, thereby facilitating the identification of desirable solutions. Figure 4 shows the Pareto front for the objectives of flow and heat transfer. The Pareto optimal points are fitted using a third-degree polynomial. Under the condition of satisfying the governing equations and constraints of the optimization problem, all the proposed optimal solutions are verified to converge. This verification process guarantees the reliability and accuracy of the optimization results.

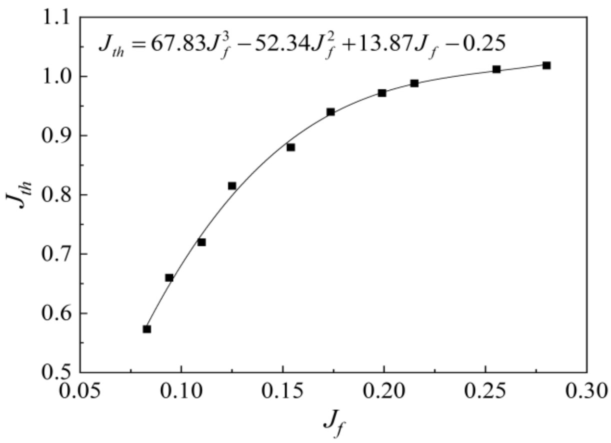

Fig. 4. Pareto front for two objectives of flow and heat transfer.

3. Simulation analysis of cold plate thermal performance

3.1. Construction of simulation model

To validate the efficiency of the topology optimization design method, the optimization result for a channel with a weighting factor w_1:w_2 = 0.7:0.3 is selected. Concurrently, a parallel flow channel cold plate is designed for comparison, ensuring that the fluid volume fraction and the length of the heat transfer boundary match those of the optimized design model. The two cold plate models are established, as illustrated in Fig. 5.

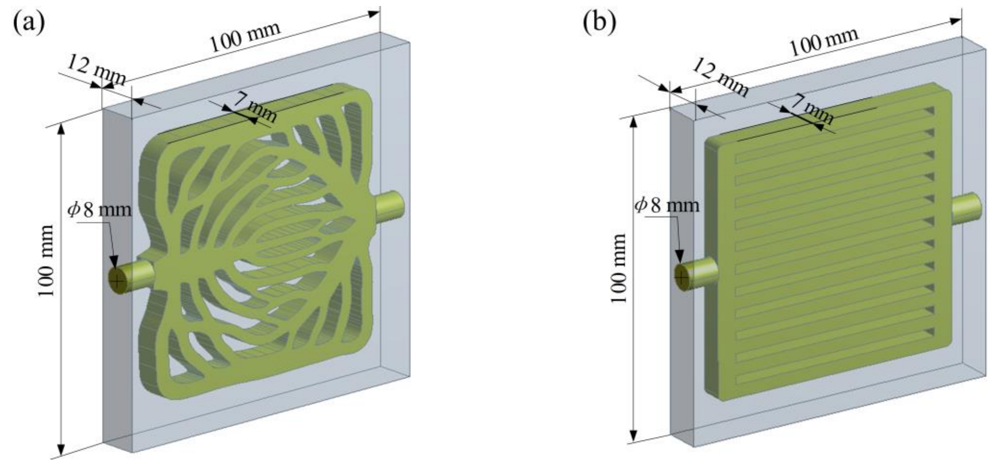

Fig. 5. Three-dimensional cold plate models of (a) topology optimization flow channel and (b) straight flow channel.

The following assumptions are made for the cold plate simulation model. Heat transfer is three-dimensional and steady-state. The fluid under consideration manifests as an incompressible laminar flow. The boundary condition attributed to the wall is that of a no-slip surface. All other wall boundaries are adiabatic except for a uniform heat source applied to the base plate. Simulations are conducted at different inlet velocities, ranging from 0.02 m/s < u_{in} < 0.22 m/s. The cold plate is fabricated using aluminum 6061, with water serving as the coolant. A reference ambient temperature is set at 20 ℃, and the outlet pressure is maintained at 0 Pa. Furthermore, a uniform heat flux of q_0 = 3.2 × 10^4 W/m^2 is supplied to the underside of the cold plate. According to the material database in COMSOL Multiphysics, the properties of both materials are detailed in Tab. 1 [23].

Table 1. Property parameters of materials.

Property parameters	Density [kgm^{-3}]	Specific heat [Jkg^{-1}K^{-1}]	Thermal conductivity [Wm^{-1}K^{-1}]	Dynamic viscosity [kgm^{-1}s^{-1}]
Aluminum 6061	2700	896	167	-
Water	998	4180	0.6	0.001

3.2. Grid independence test

To avoid numerical errors attributed to suboptimal grid quality, a grid independence test is performed. As shown in Tab. 2, four different grid partitioning schemes are used for numerical verification. Upon exceeding 864,338 grid elements, the relative errors of ΔP at the cold plate inlet and outlet, and ΔT in the system, are all observed to be less than 1%. This indicates that the simulation results are relatively independent of grid quality.

Table 2. Results of grid independence test.

Number of grids	ΔT	Relative error	ΔP	Relative error
446,139	32.7535	-	3.9832	-
563,705	33.3046	1.37%	4.0460	1.58%
634,694	33.1609	0.43%	4.1566	2.73%
864,338	33.1124	0.15%	4.1897	0.80%

3.3. Results and discussion

3.3.1 Analysis of numerical results

Figure 6 depicts the temperature distribution on the cold plate surface, as determined by simulations at an inlet velocity of 0.1 m/s. The topology-optimized model exhibits an average temperature of 44.2 ℃, a maximum surface temperature of 54.3 ℃, and a root mean square temperature of 6.2 ℃. An elliptical low-temperature zone is centered within the model. This configuration facilitates enhanced heat exchange with the low-temperature coolant over a greater solid area, resulting in more efficient thermal performance. For the parallel channel model, the average temperature stands at 47.2 °C, with a maximum temperature of 65.0 °C and a root mean square temperature of 12.6 °C. The low-temperature area presents a triangular distribution, predominantly near the inlet. Consequently, the optimized channel model significantly outperforms the parallel channel model in terms of surface temperature uniformity.

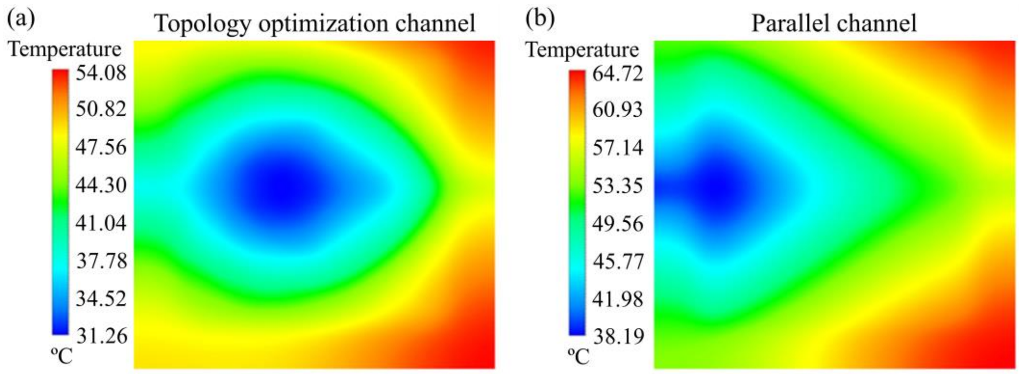

Fig. 6. Temperature distributions on the cold plate surfaces with (a) the topology-optimized channel and (b) the parallel channel configurations.

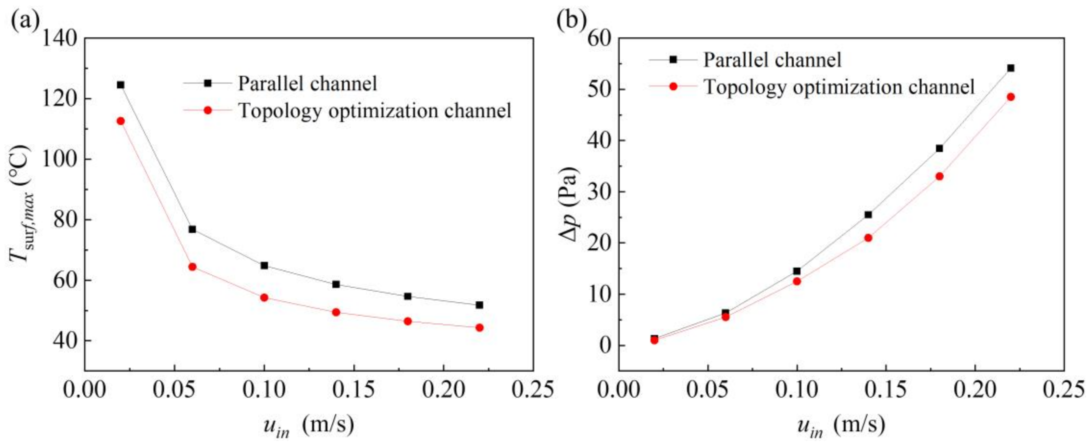

Fig. 7. Numerical simulation curves of (a) the maximum temperature on the cold plate surface and (b) the pressure drop relative to the inlet velocity.

Figure 7 shows the numerical simulation curves for maximum temperature and pressure drop relative to the inlet velocity. As the inlet flow velocity increases, the heat exchange between the fluid and the wall is further strengthened, resulting in a decreased surface temperature of the heat-generating device. At an inlet flow velocity of u_{in} = 0.18 m/s, the topology optimization model exhibits a maximum temperature approximately 15% lower than that observed in the parallel channel model. Figure 7(b) shows the curve of pressure drop variation with flow velocity. As the inlet flow velocity increases, there is a concurrent rise in the pressure drop across the channel. Nevertheless, it is essential to highlight that the pressure drop of the optimized channel consistently remains lower than that of the parallel channel structure. This underscores one of the advantages of topology optimization designs in reducing flow losses within the cold plate.

3.3.2 Thermal performance analysis

The hydrothermal capability of the cold plate is further evaluated by calculating the Nusselt number and thermal resistance. The formula for calculating the average Nusselt number Nu_{avg} is as follows:

$$Nu_{avg} = \frac{h_{avg} D_h}{k_f} \tag{17}$$

where h_{avg} represents the average heat transfer coefficient. D_h is the hydraulic diameter.

The thermal resistance R_{th} can be expressed as:

$$R_{th} = \frac{T_{surf,\max} - T_{in}}{Q_{\mathrm{w}}} \tag{18}$$

where Q_{w} is the power of the heat source.

Figure 8(a) shows the curve of Nu_{avg} changing with the inlet velocity. The analysis reveals that the parallel channel configuration exhibits a lower Nusselt number compared to the topology optimization channel. Specifically, at an inlet velocity of 0.18 m/s, the topology optimization design demonstrates the Nusselt number increase of approximately thirty percent relative to the parallel channel configuration. The enhancement in heat transfer capacity is primarily attributed to the refined branch-shaped channel topology. In the optimized design, the channel gradually splits into smaller branches from the main channel. Following adequate heat exchange with the substrate, the flow converges back into the main channel, promoting fluid cross-mixing and heat transfer to the wall.

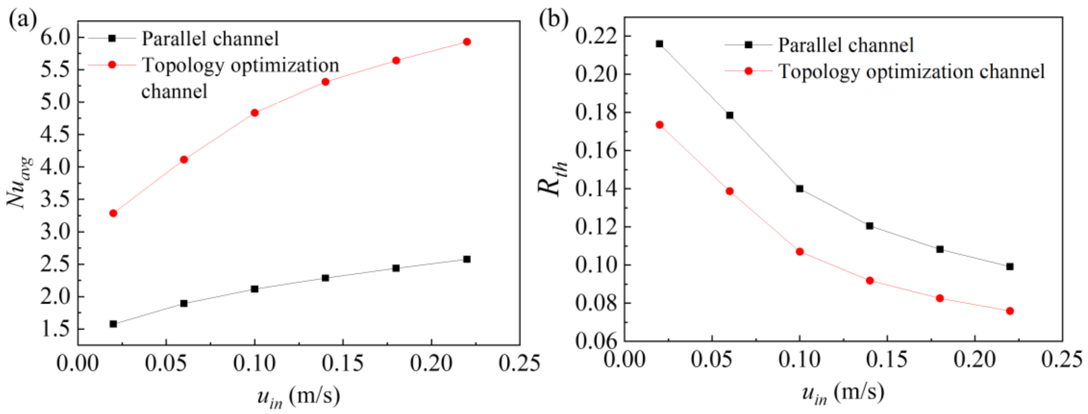

Fig. 8. Numerical simulation curves of (a) the Nusselt number Nu_{avg} and (b) the thermal resistance R_{th} versus the inlet velocity.

On the other hand, the presence of small branches and curved channels in the optimization process disrupts the flow boundary layer and diminishes its thickness, increasing the heat transfer capacity. Figure 8(b) illustrates the curve of the total thermal resistance changing with the inlet velocity. With increasing velocity, there is a noticeable trend of the total thermal resistance decreasing. The optimized design exhibits a lower total thermal resistance compared to the parallel channel design. Specifically, when u_{in} = 0.18 m/s, the topology optimization design achieves a reduction in total thermal resistance of approximately 23%.

4. Experimental verification

4.1. Manufacture of cold plate and experimental system

The material selected for the cold plate during the topology optimization process is aluminum 6061. The cold plate is partitioned into two segments for the manufacturing procedure. Annular grooves, measuring 2.8 mm by 2.6 mm in cross-section, are designed around the flow channel and filled with a silicone seal. Sealing is accomplished by fastening the extruded sealant. The cold plate inlet and outlet are connected to the pipeline using pneumatic quick connectors. An airtightness test confirmed the effectiveness of the seal. Figure 9 displays the cold plate sample.

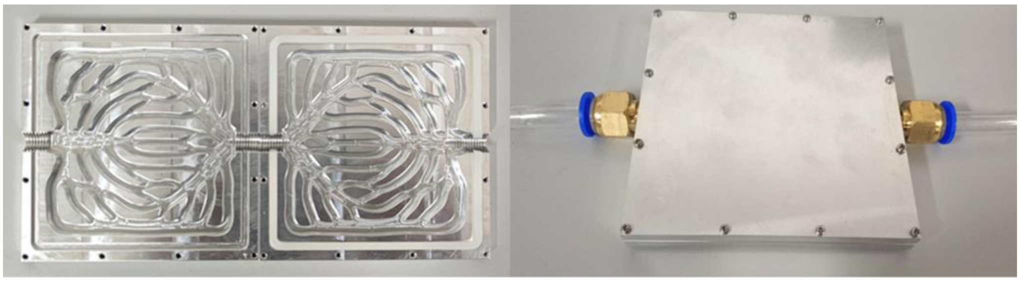

Fig. 9. The internal channel and external packaging structure of the cold plate sample.

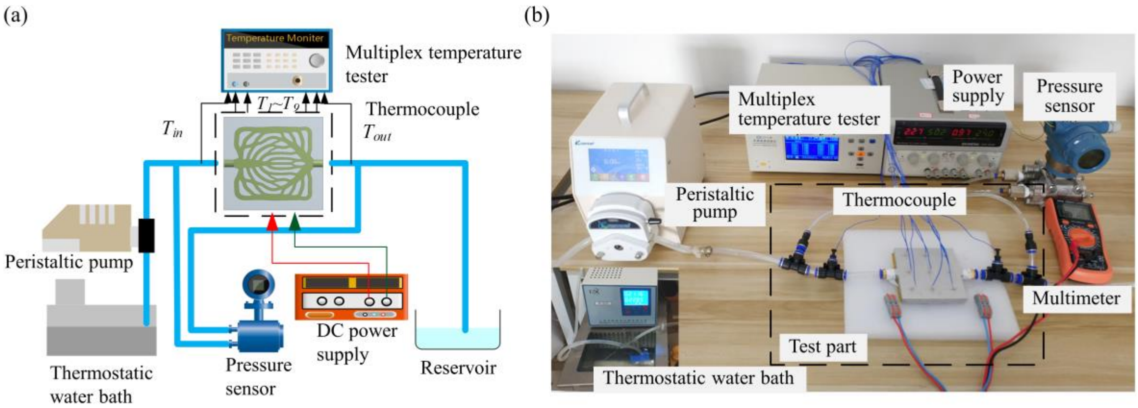

Fig. 10. Experimental system for liquid cooling of (a) the principle schematic diagram and (b) the photograph.

Figure 10 displays the experimental setup for the cold plate. In the experiment, a thermostatic water bath is used to regulate the inlet water temperature, offering a control range of -5 ℃ to 100 ℃ and a temperature control precision of ±0.05 ℃. A peristaltic pump, which can attain a maximum output flow rate of 1300 mL/min with 1% accuracy, serves as the liquid driving force. A multiplex temperature tester is employed to measure the inlet water temperature and the temperature at nine specific monitoring points. Additionally, the pressure drop across the channel of the cold plate is measured using a pressure sensor, which has a range of 0 kPa to 3 kPa and an accuracy of ±0.075%. The uniform heat source is simulated by four high-temperature ceramic heating plates with a heat flux of 3.2 W/cm^2.

4.2. Experimental results analysis

To study the hydrothermal performance at different flow velocities, the peristaltic pump is adjusted using the control panel to achieve the desired inlet velocities of u_{in} = 0.06, 0.1, 0.14, 0.18, 0.22, and 0.26 m/s. The nine temperature test points are evenly distributed on the surface of the cold plate. The above experimental scheme yields the average temperature of the measurement points and the outlet water temperature. Figure 11 shows the comparison curves of the experimental and simulation results. The graph unequivocally displays a consistent enhancement in the heat transfer capability between the fluid and the wall with increasing velocity. Consequently, the experimentally measured average temperature and the outlet water temperature exhibit a continuous decline, albeit at a diminishing rate. The experimental and simulated values show good agreement, with maximum errors of 3.07% and 3.57%, respectively. Moreover, as the flow velocity increases, the discrepancy between experimental and simulation data diminishes. The comparison of the simulation and experimental data verifies the effectiveness of the numerical analysis and proves the rationality of the topology optimization design method. These findings provide an effective reference for engineering applications.

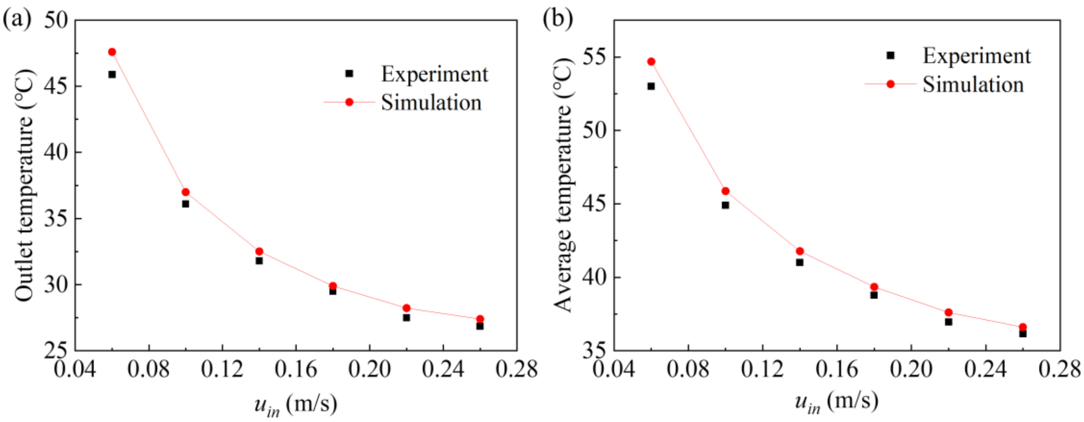

Fig. 11. Comparison curves between the experimental and simulation outcomes for (a) the outlet temperature and (b) the average temperature of the measurement points across various inlet velocities.

Due to machining errors of the sample, experimental instrument errors, and other uncertainties, the final experimental results show some deviations. The absolute machining error of the inlet channel diameter is ±0.01 mm. The relative errors of temperature mesaurement and pressure measurement are ±0.5% and ±0.2%, respectively. The relative error of the heating element power loss is ±4%, and the relative error of flow control is ±3%. To analyze the uncertainty in this experiment, the following method is used to calculate the uncertainty:

$$U_R = \sqrt{\sum_{i=1}^{i=\mathrm{N}} \left(U_{x_i} \frac{\partial R}{\partial x_i} \right)^2} \tag{19}$$

where U_R represents the absolute uncertainty of factor R, U_{x_i} denotes the uncertainty of each independent parameter, and N signifies the number of independent parameters.

It follows that the maximum relative uncertainty of the inlet velocity u_{in} can indeed be calculated to be 4.08%.

5. Conclusions

In this study, a complex mathematical model has been developed to optimize the topology of cooling channels, aiming to maximize heat transfer efficiency and minimize fluid dissipation. The density filter and projection combination method are employed to mitigate numerical instability. The efficacy of the model is demonstrated by solving the arrangement example of inlet and outlet distribution at the centerline of the cold plate, which yields a coherent and well-defined channel structure.

Optimization models under different weight combinations are solved. Through a comprehensive analysis of the pressure drop and the heat transfer boundary length, the impact of the objective function weight on the channel form is thoroughly investigated. The acquisition of the Pareto front in the topology optimization design provides designers with a range of feasible alternatives, thereby streamlining the decision-making process.

The topology optimization result, with a weighting factor of w_1:w_2 = 0.7:0.3, is selected to establish a cold plate simulation model. For comparison, a conventional parallel flow channel cold plate is designed, maintaining the same fluid volume fraction and heat transfer boundary length. The cooling performance analysis demonstrated that the topology optimization channel exhibited significantly superior cooling performance compared to the parallel flow channel.

The cold plate sample is designed and manufactured, followed by a cooling performance experiment. The results reveal that the maximum error between the simulation and the experiment is within 4%, further proving the rationality of the topology optimization design method. This research not only advances the understanding of cooling channel optimization but also offers a robust framework for the design of more efficient thermal management systems.

Acknowledgment

This work was supported by National Natural Science Foundation of China (No. 52275270), National Natural Science Foundation of China National Key R&D Plan of "Gravitational Wave Detection" Key Special Project (No. 2021YFC2203501), and Natural Science Basic Research Program of Shaanxi (No. 2023-JC-JQ-38).

References

[1] Gong, Z., *et al*., A Study of the Effects of the Micro-channel Cold Plate on the Cooling Performance of Battery Thermal Management Systems, *Thermal Science, 26* (2022), 2B, pp. 1503-1517
[2] Farhan, M., *et al*., Design and Analysis of Liquid Cooling Plates for Different Flow Channel Configurations, *Thermal Science, 26* (2022), 2B, pp. 1463-1475
[3] Xia, Y., *et al*., Numerical Investigation of Microchannel Heat Sinks with Different Inlets and Outlets Based on Topology Optimization, *Applied Energy, 330* (2023), pp. 120335
[4] Wang, J., *et al*., Study of the Influence of Objective Functions on the Topology Optimization Design of Battery Cold Plate, *Applied Thermal Engineering, 226* (2023), PP. 120326
[5] Matsumori, T., *et al*., Topology Optimization for Fluid–thermal Interaction Problems under Constant Input Power, *Structural and Multidisciplinary Optimization, 47* (2013), 4, pp. 571-581
[6] Sato, Y., *et al*., An Optimum Design Method for a Thermal-fluid Device Incorporating Multi-objective Topology Optimization with an Adaptive Weighting Scheme, *Journal of Mechanical Design, 140* (2018), 3, pp. 031402

[7] Zhao, X., *et al*., A "Poor Man's Approach" to Topology Optimization of Cooling Channels Based on a Darcy Flow Model, *International Journal of Heat and Mass Transfer, 116* (2018), pp. 1108-1123

[8] Liu, W., *et al*., Micro-channel Topology Optimization Based on Enhanced Heat Transfer Mechanism, *Thermal Science, 28* (2024), 1B, pp. 611-626

[9] Li, H., *et al.*, Experimental and Numerical Investigation of Fluid Cooling Channel Layout Designed by Topology Optimization, *Journal of Mechanical Engineering, 55* (2019), 10, pp. 198-206

[10] Zhang, T., *et al*., Topology Optimization of Regenerative Cooling Channel in Non-uniform Thermal Environment of Hypersonic Engine, *Applied Thermal Engineering, 219* (2023), pp. 119384

[11] Haertel, *et al*., Topology Optimization of a Pseudo 3D Thermofluid Heat Sink Model, *International Journal of Heat and Mass Transfer, 121* (2018), pp. 1073-1088

[12] Yaji, K., *et al*., A Topology Optimization Method for a Coupled Thermal–fluid Problem using Level Set Boundary Expressions, *International Journal of Heat and Mass Transfer, 81* (2015), pp. 878-888

[13] Pei, Y., *et al.*, Research on Air-cooled Heat Sink Based on Topology Optimization, *Journal of Mechanical Engineering, 56* (2020), 16, pp. 91-97

[14] Long, K., *et al*., Multi-material Topology Optimization for the Transient Heat Conduction Problem using a Sequential Quadratic Programming Algorithm, *Engineering Optimization, 50* (2018), 12, pp. 2091-2107

[15] Li, X., *et al.*, Multi-material Topology Optimization of Transient Heat Conduction Structure with Functional Gradient Constraint, *International Communications in Heat and Mass Transfer, 131* (2022), pp. 105845

[16] Zhou, J., *et al.*, Thermal Design of Microchannel Heat Sinks using a Contour Extraction Based on Topology Optimization (CEBTO) Method, *International Journal of Heat and Mass Transfer, 189* (2022), pp. 122703

[17] Mo, X., *et al*., Topology Optimization of Cooling Plates for Battery Thermal Management, *International Journal of Heat and Mass Transfer, 178* (2021), pp. 121612

[18] Guest, J. K., Prevost, J. H., Topology Optimization of Creeping Fluid Flows using a Darcy-Stokes Finite Element, *International Journal for Numerical Methods in Engineering, 66* (2006), 3, pp. 461-484

[19] Liu, Z., *et al*., Numerical Analysis of Topology-optimized Cold Plates for Thermal Management of Battery Packs, *Applied Thermal Engineering, 238* (2024), pp. 121983

[20] Kobayashi, H., *et al.*, Topology Design of Two-fluid Heat Exchange, *Structural and Multidisciplinary Optimization, 63* (2021), pp. 821-834

[21] Lazarov, B. S., Sigmund, O., Filters in Topology Optimization Based on Helmholtz-type Differential Equations, *International Journal for Numerical Methods in Engineering, 86* (2011), 6, pp. 765-781

[22] Wang, F., *et al*., On Projection Methods, Convergence and Robust Formulations in Topology Optimization, *Structural and Multidisciplinary Optimization, 43* (2011), 6, pp. 767-784

[23] COMSOL Multiphysics 5.4, COMSOL Inc., https://cn.comsol.com/products

[24] Schenk, O., Gartner, K., Solving Unsymmetric Sparse Systems of Linear Equations with PARDISO, *Future Generation Computer Systems, 20* (2004), 3, pp. 475-487

[25] Svanberg, K., The Method of Moving Asymptotes—A New Method for Structural Optimization, *International Journal for Numerical Methods in Engineering, 24* (1987), 2, pp. 359-373

[26] Koga, A., *et al*., Development of Heat Sink Device by Using Topology Optimization, *International Journal of Heat and Mass Transfer, 64* (2013), pp. 759-772

Submitted: 24.03.2024.
Revised: 14.07.2024.
Accepted: 22.07.2024.